Aggregation kinetics of the Aβ1-40 peptide monitored by NMR

Journal Name

COMMUNICATION

Aggregation kinetics of the Aβ1-40 peptide monitored by NMR

Giovanni Bellomo,[a] Sara Bologna,[a] Leonardo Gonnelli,[a] Enrico Ravera,[a,b] Marco Fragai,[a,b] Moreno Lelli[a,b*] and Claudio Luchinat [a,b,c*]

Received 00th January 20xx,
Accepted 00th January 20xx

DOI: 10.1039/x0xx00000x

www.rsc.org/

The aggegation of Aβ1-40 was monitored by solution NMR, which showed a trend specular to the one observed by ThT-fluorescence. The NMR data support a kinetic model where Aβ1-40 initially aggregates with the reversible formation of oligomeric species, which then irreversibly convert into fibrils.

Aβ1-40, Aβ1-42 and τ-protein are involved in the onset and progression of Alzheimer's disease (AD).[1] In particular the Aβ peptides are the major constituent of the amyloid plaques found in biopsies of AD patients. Although Aβ1-40 is the most common isoform of Aβ, Aβ1-42 seems to be more toxic and more prone to aggregation.[2] Moreover, The structure of the final fibrillary aggregates of Aβ1-40[3,4] is found to be different from the one of Aβ1-42[5–7]and not univocal.[8] There are also evidences that the structure of the transient oligomeric species might be different between the two isoforms, with Aβ1-42 forming more fibril-like oligomers, rich in β-sheets, and Aβ1-40 forming more globular and amorphous aggregates.[9–11] The soluble oligomers and especially the low molecular weight (LMW) oligomers showed to be the most toxic species among all the Aβ aggregates.[12,13] These findings suggest that the aggregation kinetics may be different for the two isoforms of Aβ as proposed in some of the kinetic models developed over the years.[14–18] The development of kinetic models and the understanding of the aggregation mechanisms of amyloidogenic proteins would be dramatically important in designing new therapies and drugs. In 2011 Knowles and co-workers[17] developed a two-species (monomers and fibrils) model for describing the aggregation of Aβ1-42. They also introduced the idea of surface-catalysed secondary nucleation[19] and tested the model against ThT fluorescence data at different monomer concentrations.[20] The model was then adapted[18] to Aβ1-40, observing strong differences in nucleation behaviour and suggesting that secondary nucleation saturates above 6 μM of Aβ1-40 monomer concentration. However, Kelly and co-workers[21] brought up evidences of conversion of soluble globular oligomers of Aβ1-40 into fibrils; this evidence was also supported by other works.[22–24] These findings suggest that considering only two species for the kinetic modelling of amyloid aggregation, at least for Aβ1-40, could be reductive. For this reason, we investigated the aggregation kinetics of Aβ1-40 by solution NMR, focusing our attention on the early stage of the aggregation. The peculiarity of NMR is that it monitors directly the free monomer concentration, which is affected from the beginning of the aggregation process, thus providing complementary information with respect to ThT-fluorescence. With modern high-field instruments the NMR experiments can be performed under near physiological conditions, at micromolar concentration range, and without the need to add fluorescent or chromophoric probes that may alter the aggregation.[25] Solution NMR was already applied to study the aggregation of the Aβ peptides: Fawzi *et al.*[26,27] obtained information about oligomeric species of Aβ1-40/42 using the dark-state exchange saturation transfer (DEST), probing the exchange processes between monomers and protofibril-bound states. Pauwels *et al.*[28] and Bax and coworkers[29] monitored the Aβ1-40/42 aggregation with NMR and ThT-fluorescence but they did not propose kinetic models for the amyloidogenic process. Ramamoorthy and coworkers obtained an high resolution structure of a partially folded Aβ1-40 monomer with solution NMR[30] and observed directly the formation of at least five different oligomeric species by using ^{19}F-NMR on a ^{19}F labelled Aβ1-40 peptide.[31] They also further characterized some oligomeric aggregates with solid-state NMR in a subsequent work.[32] Oligomerization kinetics was monitored also by Bertini and co-workers with sedimentation NMR,[9,33] trapping oligomeric species of about 70-80 kDa by MAS induced

[a] *Magnetic Resonance Center (CERM), University of Florence, Via L. Sacconi 6, 50019 Sesto Fiorentino, Italy. Email: lelli@cerm.unifi.it, luchinat@cerm.unifi.it*
[b] *Department of Chemistry "Ugo Schiff", University of Florence, Via della Lastruccia 3, 50019 Sesto Fiorentino, Italy.*
[c] *Giotto Biotech S.R.L., Via Madonna del Piano 6, 50019 Sesto Fiorentino, Florence, Italy.*

† Footnotes relating to the title and/or authors should appear here.
Electronic Supplementary Information (ESI) available: supporting figures, mathematical description of kinetic models, experimental details. See DOI: 10.1039/x0xx00000x

sedimentation. In order to obtain information about the aggregation kinetics of Aβ1-40 we acquired a series of 1D ^{1}H NMR spectra in quiescent condition. The NMR investigation was performed on recombinant Aβ1-40 samples at pH 8.5 and with concentrations between 30 and 100 μM, for details see the supporting information (SI). This higher than physiological pH was chosen because it corresponds to the pH where Aβ1-40 easily form fibrils with high reproducibility.[3] The temperature was set to the physiological value of 310 K in order to avoid a too long lag-time, considering that the elongation rate of amyloids strongly increases with temperature,[34] while lower temperatures can promote a partially folded state of the monomer.[30] In Figure 1 we report the trend of the methyl region of the 1D ^{1}H spectrum as a function of time up to the almost complete disappearance of the monomer resonances. The intensities of the methyl peaks decreased with an almost sigmoidal behaviour with a slow decrease in monomer concentration of about 10% during the first 20 hours; then a sharp concentration decrease is observed, with the consumption of most of the monomer, followed by a final plateau where the monomer concentration remained almost stationary at less than 2% of the initial amount. Similar trends were observed also for the aromatic resonances (see SI, Fig. S3) but we analysed the methyl region because of the higher signal to noise ratio.

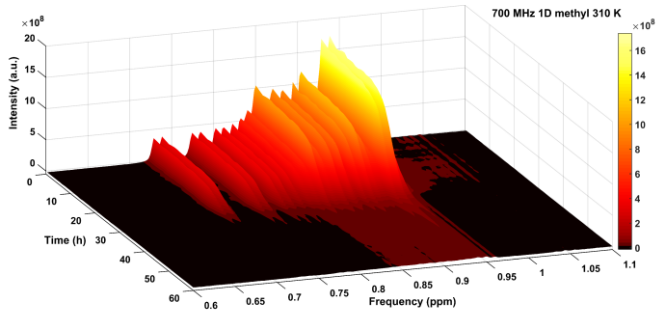

Figure 1: Series of 1D ^{1}H NMR spectra of the methyl region of a 50 μM sample of Aβ1-40 plotted with MATLAB. Spectra were acquired with a 700 MHz (16.4 T) spectrometer, using an ammonium acetate buffer at pH 8.5 (see details in the SI). Spectra were binned with AMIX software (bin width = 0.005 ppm) prior to image formation.

To get insight about this process, we repeated the aggregation experiment by monitoring another 50 μM Aβ1-40 sample simultaneously through NMR and ThT fluorescence. Figure 2 reports the NMR integral of the methyl region as a function of time compared with the increase of the fluorescence signal. The presence of ThT can affect the kinetics of the fibril formation, especially with ThT concentration comparable to the Aβ1-40 concentration.[25] Thus we kept the ThT concentration at 5 μM (1/10 of the Aβ1-40 concentration) and we added it in both the NMR tube and the quartz cuvette. Notably, the drop of the monomer concentration happens in concomitance with the growth of the fluorescence (due to fibril formation), with an almost specular trend. The NMR experiments were repeated at different initial monomer concentrations (30, 50 and 100 μM) in order to understand the impact of the concentration on the aggregation kinetics. The decrease of the integrals of the methyl spectrum as a function of time is reported in Figure 3 and is almost entirely associated to the monomer consumption (see SI and Fig. S1). We fitted these experimental data using three different kinetic models. In Figure 3A the NMR integrals are fitted with the model developed by Knowles and coworkers.[18] This model was created also considering the previous works of Oosawa,[35] Ferrone,[16] Murphy[17] and Pöschel.[36] In this two-species model, the monomeric Aβ is expected to nucleate directly to fibrils, which in turn can elongate, dissociate or fragment into shorter fibrils.

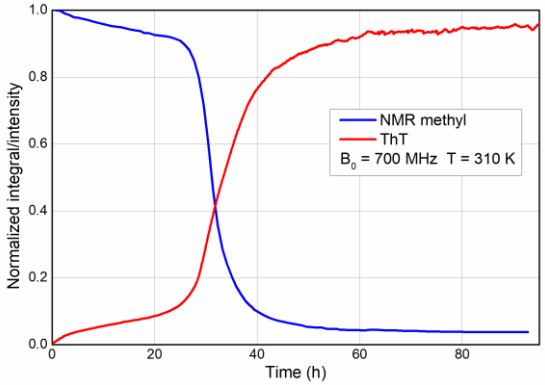

Figure 2: Aggregation kinetics of 50 μM of Aβ1-40 at 310 K and pH 8.5. The decrease of the methyl proton integral showed a behaviour complementary to the ThT fluorescence intensity. NMR integrals were normalized by dividing them by the highest value, ThT fluorescence data were normalized setting the point at 92.8 h to 1–(the NMR normalised integral) in that point.

Secondary nucleation catalysed by the fibril surface is also included, as it was demonstrated to have a key role in Aβ1-42. This model was adapted[19] to the aggregation trend of Aβ1-40 at pH 7.4, introducing a saturation limit for the secondary nucleation for Aβ1-40 monomer concentration: the results of the fitting to this model are shown in Figure 3B. In Figure 3A and 3B the simulated curves reproduce the sigmoidal-like decrease at the main inflection point, but the agreement is rather poor for the initial part of the trend. We thus decided to modify the model of Knowles considering also the formation of oligomeric species. In our model (depicted in Fig. S4 and Eq. S1 and S2 in the SI), monomers can nucleate into oligomers, the nucleation kinetics considered being fundamentally equal to the one used by Knowles,[18] Ferrone,[16] Pöschel[36] and to the one originally developed by Oosawa.[35] In our case, however, monomers do not nucleate directly into fibrils but into transient oligomeric aggregates. Oligomers can grow and decrease by addition or dissociation of monomers, as well as fibrils, but with different kinetic rates with respect to the latter. For the depolymerization kinetics we used slightly different terms in the kinetic equations resulting in a total probability of monomer detachment proportional to the oligomer size (see SI). The crucial part of the model is the introduction of a conversion kinetics step from oligomers to fibrils: when the oligomers reach a given critical size n_c (e.g. 20 monomers in the present case) they are allowed to irreversibly convert into fibrils. Fibrils can then grow and decrease through polymerization and depolymerization by addition or release of monomers with a kinetics identical to the one of the previously cited models.[15,16,20,35,36] Likewise, fibrils

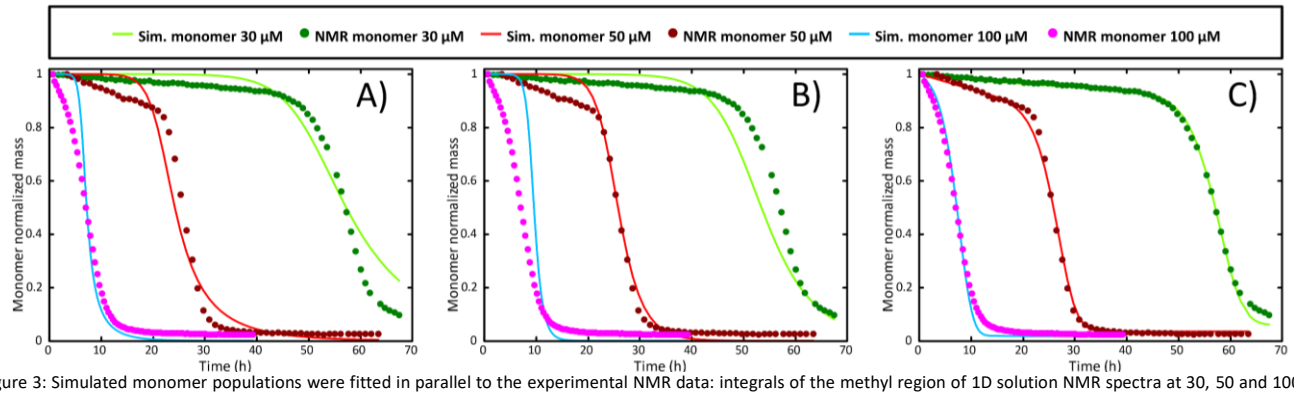

Figure 3: Simulated monomer populations were fitted in parallel to the experimental NMR data: integrals of the methyl region of 1D solution NMR spectra at 30, 50 and 100 µM Aβ1-40 initial monomer concentration (pH 8.5, T=310 K). Three different kinetic models were tested on these data: In A) the two-species model for Aβ1-42, in B) the two-species model for Aβ1-40 while in C) the "conversion" model developed in this work.

can also fragment producing smaller fibrils (not oligomers or monomers) that can then act as new seeds for polymerization. In this model fibrils are not allowed to fragment in species smaller than the critical size n_c. In this way, fragmentation of fibrils only produces fibrils above the critical size and this is why we named this process "fibril closed fragmentation". With this kinetic model we fitted the experimental data in Figure 3C. The addition of the irreversible conversion from oligomers into fibrils allowed for a significantly better agreement between the simulated and the experimental data with respect to the previous models, especially for the initial part of the aggregation. Notably, this model fits well the evolution during the lag-time were oligomers are supposed to be formed; by NMR we can monitor this evolution through the monomer consumption while the fluorescence remains quite low. The fitted kinetic constants of the three tested models are shown in Table S1 in the SI. In our "conversion model" the kinetic constant for the fibril growth (k_+) is an order of magnitude higher than the one for the monomer addition to oligomeric species (k_{+ol}). This difference explains why, once a sufficient amount of large oligomers is converted to fibrils, monomers start to be rapidly consumed while the mass of fibrils rapidly increases producing a sigmoidal-like behaviour for the monomer consumption kinetics. In the third part of the trend, in the tail of the sigmoidal decrease, where most of the peptides are aggregated into fibrils, the process of monomer dissociation remains the only relevant, and is responsible for the residual amount of monomer still present in solution. In the previously published models for Aβ1-40[19] and Aβ1-42[18] there is no distinction between "oligomers" and "fibrils" and a single polymerization constant is fitted for all the aggregation steps. With these models the rapid monomer consumption of the sigmoidal trend is the result of a strong secondary nucleation that becomes explosively strong as soon as there is a small amount of long-fibrils formed. On the basis of the fitted kinetic constants we back-calculated the relative fibril size distribution for the three models (Figure S7, S8 and S9). With reference to Figure S7 (50 µM sample) for the Aβ1-42 and Aβ1-40 models it results that, at the end of the aggregation process (t ~60h), the majority of the fibrils should have a size smaller than 20 monomers, and for the Aβ1-42 model even smaller than 10 monomers (40 kDa). In the trials we made, only the model based on the oligomer-to-fibril conversion predicts the formation of fibrils larger than 433 kDa (>100mers). Indeed, the strong secondary nucleation process of the first two models results in a rapid formation of dimers during the sigmoidal step that are not able to elongate much because of the depleted monomer concentration in solution. In our conversion model we have not included secondary nucleation and the "limited" number of converted fibrils favours their elongation towards high molecular weights. We do not exclude that the secondary nucleation process exists for Aβ1-40, since it has been well demonstrated for Aβ1-42,[21] but for Aβ1-40 in our conditions of concentration and pH (8.5), the secondary nucleation seems not to be determinant. Indeed, if secondary nucleation is included into the conversion model (Figure S5 and Table S2), its impact on the fit quality is minimal and the relative kinetic constant remains quite small. Solution NMR is a profitable technique to follow these aggregation processes, because it gives an overview of the sample status. In several cases, the presence of impurities or the concomitant occurrence of degradation processes (for example due to undetectable amounts of proteases[37]) can be determined by 1D ^{1}H NMR spectra. In the SI we report the case of degradation (Fig S10), which usually manifests itself with the formation of sharp resonances near the ones of the monomer. Another aspect which needs attention is

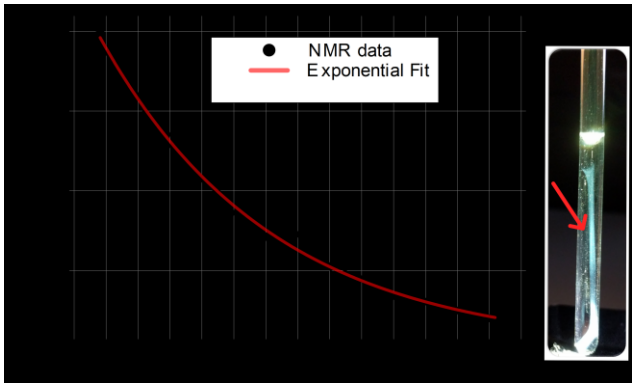

Figure 4: A) The kinetic profile of the NMR signal (B_0 = 700 MHz T= 310 K) was fitted with an exponential decay that is typical of a polymerization kinetics. B) Curious image of an agglomerate of fibrils presumably grown over the surface of an impurity present in the bottom of the NMR tube, the pale blue color resulted from the addition of 5 µM of ThT.

the presence of preformed aggregates and/or electrostatic surfaces that can drastically promote fibrillation *in vitro*.[38] As an example, in Fig. 4 we show a sample where presumably the

presence of a solid impurity promoted the formation of a macroscopic fibrillary aggregate into the NMR tube. The presence of this impurity had a dramatic effect on the aggregation kinetics. Some fibrillary nuclei were formed on its surface at the bottom of the NMR tube. From these quickly formed nuclei the aggregation proceeded mainly through polymerization. This hypothesis is also in line with the observation of an exponential decay of the monomer signal (Fig. 4B). Indeed, with reference to Eq. S6, a pure polymerization kinetics from a preformed concentration of fibrils implies an exponential decay of the monomer.

In conclusion, solution NMR is a valuable technique for the investigation of the aggregation kinetics of the Aβ1-40 peptide, giving a complementary point of view compared to ThT fluorescence. We developed a computational model that well fits the trend of the monomer consumption and supports the existence of at least two categories of aggregates: oligomers and fibrils, with different rates of growth. Despite the existence of oligomeric and fibrillar species in Aβ1-40 aggregation is a well-established concept, the quantification of the aggregation rates involving these species and the development of a reliable computational model is an important step forward for the comprehension of Aβ aggregation processes. Furthermore, it makes possible to quantify the actual impact of drug candidates in contrasting aggregation and protein misfolding.

This work was supported by ERA-NET NEURON ABETA ID, MIUR PRIN 2012SK7ASN, Fondazione Cassa di Risparmio di Firenze, the University of Florence CERM-TT and Instruct-ERIC, an ESFRI Landmark, supported by national member subscriptions. Specifically, we thank the Instruct-ERIC Core Centre CERM, Italy.

Conflicts of interest

There are no conflicts to declare.

Notes and references

1 J. Wang, B. J. Gu, C. L. Masters and Y.-J. Wang, *Nat. Rev. Neurol.*, 2017, **13**, 612–623.
2 K. Parameshwaran, C. Sims, P. Kanju, T. Vaithianathan, B. C. Shonesy, M. Dhanasekaran, B. A. Bahr and V. Suppiramaniam, *Synap. N. Y. N*, 2007, **61**, 367–374.
3 I. Bertini, L. Gonnelli, C. Luchinat, J. Mao and A. Nesi, *J. Am. Chem. Soc.*, 2011, **133**, 16013–16022.
4 J.-X. Lu, W. Qiang, W.-M. Yau, C. D. Schwieters, S. C. Meredith and R. Tycko, *Cell*, , DOI:10.1016/j.cell.2013.08.035.
5 Y. Xiao, B. Ma, D. McElheny, S. Parthasarathy, F. Long, M. Hoshi, R. Nussinov and Y. Ishii, *Nat. Struct. Mol. Biol.*, 2015, **22**, 499–505.
6 M. A. Wälti, F. Ravotti, H. Arai, C. G. Glabe, J. S. Wall, A. Böckmann, P. Güntert, B. H. Meier and R. Riek, *Proc. Natl. Acad. Sci. U. S. A.*, 2016, **113**, E4976–E4984.
7 M. T. Colvin, R. Silvers, Q. Z. Ni, T. V. Can, I. Sergeyev, M. Rosay, K. J. Donovan, B. Michael, J. Wall, S. Linse and R. G. Griffin, *J. Am. Chem. Soc.*, 2016, **138**, 9663–9674.
8 R. Tycko, *Protein Sci. Publ. Protein Soc.*, 2014, **23**, 1528–1539.
9 I. Bertini, G. Gallo, M. Korsak, C. Luchinat, J. Mao and E. Ravera, *Chembiochem Eur. J. Chem. Biol.*, 2013, **14**, 1891–1897.
10 C. G. Glabe, *J. Biol. Chem.*, 2008, **283**, 29639–29643.
11 N. J. Economou, M. J. Giammona, T. D. Do, X. Zheng, D. B. Teplow, S. K. Buratto and M. T. Bowers, *J. Am. Chem. Soc.*, 2016, **138**, 1772–1775.
12 D. M. Walsh, I. Klyubin, J. V. Fadeeva, W. K. Cullen, R. Anwyl, M. S. Wolfe, M. J. Rowan and D. J. Selkoe, *Nature*, 2002, **416**, 535–539.
13 S. Lesné, M. T. Koh, L. Kotilinek, R. Kayed, C. G. Glabe, A. Yang, M. Gallagher and K. H. Ashe, *Nature*, 2006, **440**, 352.
14 J. P. Bernacki and R. M. Murphy, *Biophys. J.*, 2009, **96**, 2871–2887.
15 F. Ferrone, *Methods Enzymol.*, 1999, **309**, 256–274.
16 M. M. Pallitto and R. M. Murphy, *Biophys. J.*, 2001, **81**, 1805–1822.
17 S. I. A. Cohen, M. Vendruscolo, M. E. Welland, C. M. Dobson, E. M. Terentjev and T. P. J. Knowles, *J. Chem. Phys.*, 2011, **135**, 065105.
18 G. Meisl, X. Yang, E. Hellstrand, B. Frohm, J. B. Kirkegaard, S. I. A. Cohen, C. M. Dobson, S. Linse and T. P. J. Knowles, *Proc. Natl. Acad. Sci. U. S. A.*, 2014, **111**, 9384–9389.
19 S. Linse, *Biophys. Rev.*, 2017, **9**, 329–338.
20 S. I. A. Cohen, S. Linse, L. M. Luheshi, E. Hellstrand, D. A. White, L. Rajah, D. E. Otzen, M. Vendruscolo, C. M. Dobson and T. P. J. Knowles, *Proc. Natl. Acad. Sci.*, 2013, **110**, 9758–9763.
21 J. Lee, E. K. Culyba, E. T. Powers and J. W. Kelly, *Nat. Chem. Biol.*, 2011, **7**, 602–609.
22 Z. Fu, D. Aucoin, J. Davis, W. E. Van Nostrand and S. O. Smith, *Biochemistry (Mosc.)*, 2015, **54**, 4197–4207.
23 M. Cheon, C. K. Hall and I. Chang, *PLoS Comput. Biol.*, 2015, **11**, e1004258.
24 N. Benseny-Cases, M. Cócera and J. Cladera, *Biochem. Biophys. Res. Commun.*, 2007, **361**, 916–921.
25 M. D'Amico, M. G. Di Carlo, M. Groenning, V. Militello, V. Vetri and M. Leone, *J. Phys. Chem. Lett.*, 2012, **3**, 1596–1601.
26 N. L. Fawzi, J. Ying, R. Ghirlando, D. A. Torchia and G. M. Clore, *Nature*, 2011, **480**, 268–272.
27 N. L. Fawzi, J. Ying, D. A. Torchia and G. M. Clore, *Nat. Protoc.*, 2012, **7**, 1523–1533.
28 K. Pauwels, T. L. Williams, K. L. Morris, W. Jonckheere, A. Vandersteen, G. Kelly, J. Schymkowitz, F. Rousseau, A. Pastore, L. C. Serpell and K. Broersen, *J. Biol. Chem.*, 2012, **287**, 5650–5660.
29 J. Roche, Y. Shen, J. H. Lee, J. Ying and A. Bax, *Biochemistry (Mosc.)*, 2016, **55**, 762–775.
30 S. Vivekanandan, J. R. Brender, S. Y. Lee and A. Ramamoorthy, *Biochem. Biophys. Res. Commun.*, 2011, **411**, 312–316.
31 Y. Suzuki, J. R. Brender, M. T. Soper, J. Krishnamoorthy, Y. Zhou, B. T. Ruotolo, N. A. Kotov, A. Ramamoorthy and E. N. G. Marsh, *Biochemistry (Mosc.)*, 2013, **52**, 1903–1912.
32 S. A. Kotler, J. R. Brender, S. Vivekanandan, Y. Suzuki, K. Yamamoto, M. Monette, J. Krishnamoorthy, P. Walsh, M. Cauble, M. M. B. Holl, E. N. G. Marsh and A. Ramamoorthy, *Sci. Rep.*, 2015, **5**, 11811.
33 I. Bertini, C. Luchinat, G. Parigi and E. Ravera, *Acc. Chem. Res.*, 2013, **46**, 2059–2069.
34 Y. Kusumoto, A. Lomakin, D. B. Teplow and G. B. Benedek, *Proc. Natl. Acad. Sci.*, 1998, **95**, 12277–12282.
35 F. Oosawa and M. Kasai, *J. Mol. Biol.*, 1962, **4**, 10–21.
36 T. Pöschel, N. V. Brilliantov and C. Frömmel, *Biophys. J.*, 2003, **85**, 3460–3474.
37 T. Saido and M. A. Leissring, *Cold Spring Harb. Perspect. Med.*, , DOI:10.1101/cshperspect.a006379.
38 B. Moores, E. Drolle, S. J. Attwood, J. Simons and Z. Leonenko, *PLoS ONE*, , DOI:10.1371/journal.pone.0025954.

